# Dynamic characterisation of MEMS using Raman spectroscopy

**Z. X. Hu[1], J. Hedley[1], B. J. Gallacher[1], I. Arce-Garcia[2]**
[1]Mechanical & Systems Engineering, Newcastle University, Newcastle upon Tyne, NE1 7RU, UK.
[2]INEX, Newcastle University, Newcastle upon Tyne, NE1 7RU, UK.

Email: John.Hedley@ncl.ac.uk

**Abstract**
This paper reports on utilising Raman spectroscopy to characterise the motion and measure strain levels in dynamic micromechanical structures. The main advantages of such a technique is that surface features are not required to characterise the 3D motion as the crystal lattice is used as the reference frame and that it is suited to high frequency measurements. Two methodologies are presented. The first utilises a strobed diode laser probe beam with the centre position of the Raman peak giving a measure of strain as a function of phase. A measurement resolution of 210 μstrain is obtained at frequencies up to 100 KHz. The second method uses a HeNe laser probe beam with the broadening of the Raman peak indicating strain levels. Although no phase data is available in the latter technique, the technique is rapid and may be utilised on a Raman system without any modification. A measurement resolution of 30 μstrain is achieved and strain mapping of a region may be performed within minutes. As strobing is not used here, the technique is not frequency limited. Comparisons with alternative optical characterisation techniques are made.

**Keywords -** MEMS characterisation; Raman spectroscopy; strain mapping

## 1. Introduction
The development of methodologies to characterise the static and dynamic properties of micro and nanoscale devices are recognized as important. They enable faster development times by identifying fabrication problems and assessment of device performance. The ideal features required by such characterisation methods are highlighted by Bosseboeuf [1], these include full 3 dimensional measurement capabilities and high measurement bandwidth. Over the last decade, significant advances on MEMS characterisation techniques have been made.

Optical techniques provide a non contact method for such characterisation, examples of which include laser vibrometer [2], stroboscopic imaging [3], interferometry [4], electronic speckle pattern interferometry (EPSI) [5], laser holography [6] and blur-synthesis [7]. Each has particular advantages in characterising the device, such as high sensitivity (~10pm for [2]), large field of view [3-7] and unlimited bandwidth [7], and associated disadvantages. Utilising several of these techniques combines these advantages [8] and allows for full 3 dimensional characterisation [9], such systems now being commercially available. In addition, these techniques are utilised for reliability studies in which they are used to give an indication of the mechanism of device failure once it has occurred or to monitor a device designed to fail at a certain point [10].

Raman spectroscopy is a technique that is being increasingly used to characterize MEMS and has the potential to offer additional advantages to the MEMS characterisation community. The profile of the Raman peak in silicon may be used to determine the material properties; the profile's peak position gives a measure of strain within the lattice whilst the profile width indicates crystallinity. Analysis of the peak position has been applied to measure strain induced from a variety of sources. It has been utilised to investigate local mechanical stress in integrated circuits due to stress inducing fabrication steps [11] and through indentation experiments of the silicon lattice [12]. For MEMS, Raman spectroscopy was shown to measure stress induced through doping [13] and via static mechanical loading of a device [14, 15]. High spatial resolution mapping is also possible, as shown

by Webster et al [16], who investigated plastically deformed regions of a silicon wafer via near-field Raman spectroscopy.

Recently, Xue et al [17] demonstrated the feasibility of utilizing Raman spectroscopy to characterize the dynamic motion of MEMS. In this work, an electro-optic modulator was used to strobe the beam of an $Ar^+$ laser to a 1% duty cycle with an on:off extinction ratio of 50:1. 30 second point measurements were taken at the base of a polysilicon microresonator operating at 10 KHz. Stresses of up to 490 ± 10 MPa were measured. An alternative method of monitoring the dynamic behaviour of MEMS was reported by Hedley et al [18]. In this work, the broadening of the Raman peak during an in plane vibration of 101 KHz was monitored. With the technique being reasonably fast (1 second per data point), strain mapping becomes feasible.

The work presented here looks at these two methodologies for utilising Raman spectroscopy as a way to characterise dynamic MEMS and give a measure of strain. The first extends the technique demonstrated by Xue et al to higher frequencies utilising a current modulated diode laser whilst the second looks at extending the analysis of the time averaged Raman signal to map the strain contours for both in plane and out of plane resonant modes. A series of test structures, as shown in figure 1, were used to assess the accuracy and repeatability of both techniques.

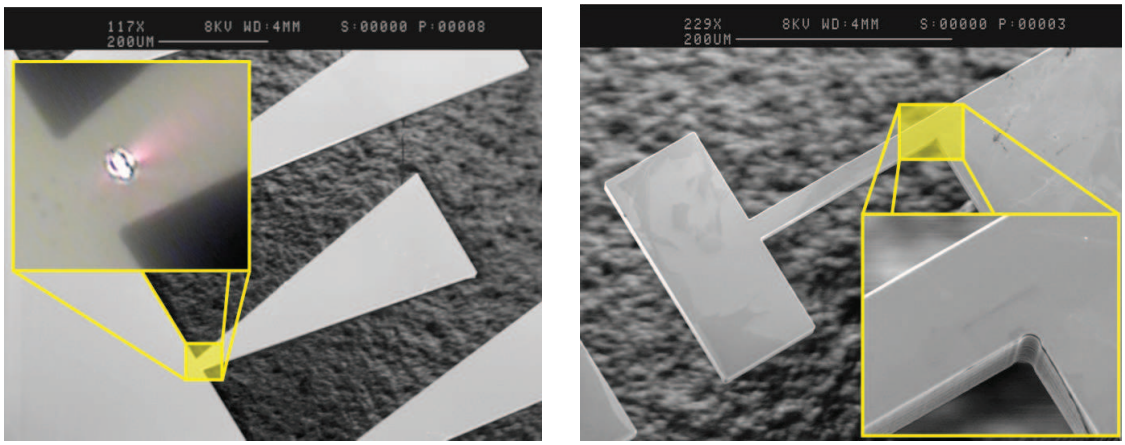


**(a)** **(b)**

Figure 1: SEM images of the fabricated cantilever type test structures. The laser position for the experimental results in section 4 is highlighted in (a). The region mapped in section 5 is highlighted in (b).

## 2. Theory

### *2.1. Raman*

The crystalline structure of silicon has a cubic diamond lattice belonging to the $O_h$ point group with Raman tensors, $R_j$, given by [19]:

$$TO_x = \begin{pmatrix} 0 & 0 & 0 \\ 0 & 0 & d \\ 0 & d & 0 \end{pmatrix}, \quad TO_y = \begin{pmatrix} 0 & 0 & d \\ 0 & 0 & 0 \\ d & 0 & 0 \end{pmatrix}, \quad LO_z = \begin{pmatrix} 0 & d & 0 \\ d & 0 & 0 \\ 0 & 0 & 0 \end{pmatrix}. \qquad (1)$$

For unstrained silicon, this triply degenerate Raman peak is centred on 520.8$cm^{-1}$. Strain within the lattice breaks this degeneracy and shifts the peak [20], tension causing the peaks to move to lower wavenumber. The contribution to the total Raman intensity from each peak is given by:

$$I = \left| p_s R_j p_i \right|^2 \tag{2}$$

where $p_i$ and $p_s$ are the polarizations of the incident laser and collected scattered photons respectively. By utilising particular crystal orientations and monitoring various scattering polarizations, a quantitative measure may be made all of unknown stress states [21]. For this work, a <100> silicon wafer was used, the incident laser polarization was (100) and all backscattered light was collected. Therefore for this geometry, only the longitudinal $LO_z$ peak is observed. During device vibration, the silicon lattice is cyclically placed under compression and tension and thus a measure of this dynamic strain may be used to characterise motion of the device.

An absolute value of strain is determined by correlating the shift in peak wavenumber with the actual strain present. This shift corresponds to the volumetric strain of the unit cell, as shown by Anastassakis et al [20]. A previous experiment which loaded a silicon wafer via a four point bending experiment determined this calibration factor to be $5.2\times10^{-4}$ $cm^{-1}$/volumetric μstrain for the $LO_z$ photon [14].

*2.2. Device modelling*

The theoretical strain in the devices was considered using two different approaches. A simple analytical model is used to give an estimate of the volumetric strain whilst finite element modelling better accounts for fabrication tolerances.

*2.2.1. Analytical model of device*

The device shown in figure 1(b) may be modelled as a cantilever with large end mass as shown in figure 2. During in plane bending, the cantilever undergoes a curvature of $K$. If $y_0$ is the position of a longitudinal fibre relative to the neutral axis, the axial strain $\varepsilon_{xx}$ in this fibre is given by:

$$\varepsilon_{xx} = y_0 K \,. \tag{3}$$

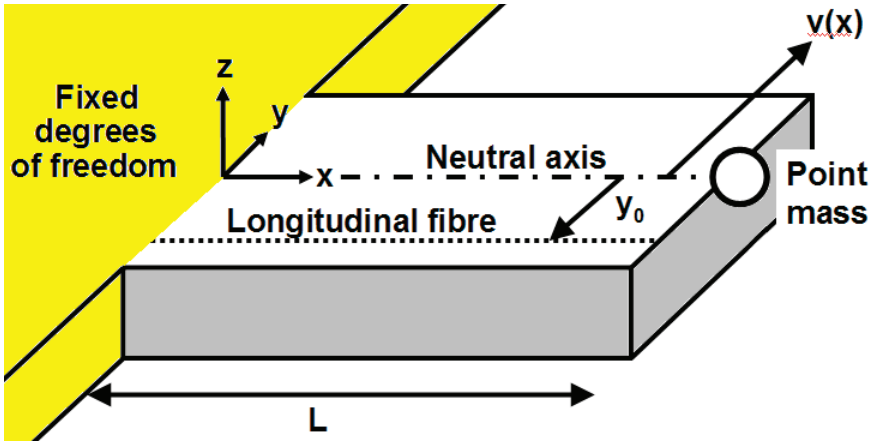


Figure 2: Schematic model of the device shown in figure 1(b).

For large deflections, this beam curvature $K$ is given by:

$$K = \frac{v'(x)}{\left[1 + v''(x)^2\right]^{3/2}} \tag{4}$$

where $v(x)$ is the deflection of the neutral axis. For this work, the beam resonates at its fundamental frequency. $v(x)$ may therefore be written in terms of the fundamental mode shape $X(x)$:

$$v(x) = \lambda X(x) \tag{5}$$

where $\lambda$ is the amplitude scaling factor and has a magnitude of 0.5 of the free end amplitude. Using Rayleigh's method [22], an approximate expression for the mode shape *X(x)* is determined:

$$X(x) = \left(\frac{L-x}{L}\right)^3 - 3\left(\frac{L-x}{L}\right) + 2. \tag{6}$$

Poisson's ratio is used to calculate the remaining principle strain components, the volumetric strain then being given by:

$$\varepsilon = \varepsilon_{xx} + \varepsilon_{yy} + \varepsilon_{zz}. \tag{7}$$

A stress concentration is expected at the clamped corner of the cantilever. The strain components are expected to increase in this vicinity by a factor of 2 for the measured fillet radius of 1μm [23]. A similar argument is applied to out of plane motions.

*2.2.2. Finite element analysis of device*

The software package ANSYS was used to model the device and surrounding support silicon using a 3D anisotropic structural solid element. The resonance frequencies were calculated and then the support region forced harmonically to give a device free end deflection comparable to the measured values on the actual devices for the vibration modes of interest. From this, volumetric strain was calculated for the region of interest.

## 3. Fabrication

A series of cantilever type test structures were fabricated from crystalline silicon to assess the suitability of Raman spectroscopy for device characterisation. Although the technique is not limited to crystalline silicon, the sharp Raman peak obtained from the crystal lattice gives a suitable profile from which to develop the technique. The structures were designed with fundamental resonant frequencies ranging from 10 KHz to 1 MHz thus allowing parallel characterisation of the devices using laser vibrometry and dynamic surface profilometry facilities available within the lab.

Test structures were fabricated out of <100> so that for the experimental geometry used, only one Raman transition was observed. It was estimated that an amplitude of several microns would be required to obtained a measurable Raman shift and so the die was design to allow for this motion both in and out of plane. To facilitate the potentially large out of plane amplitude vibrations, the handle silicon had to be removed from the device locations.

The fabrication procedure was as follows and was performed at INEX within Newcastle University. The <100> SOI wafers used were composed of a 15μm device layer, 2μm sacrificial buried oxide (BOX) layer and 500μm of handle silicon. In preparation for the DRIE (deep reactive ion etch) of the handle, the first step was to deposit an oxide layer onto the back of the SOI wafer followed by photolithography, a plasma etch of this oxide layer and removal of the remaining photoresist. Next, a photolithography and a DRIE step (stopping at the BOX layer) were performed on the front side of the wafer to pattern the device geometry. After this etch, a protective layer was placed on the device side of the SOI and a 'support' wafer bonded to this surface. A DRIE was then performed on the previously masked handle silicon followed by a plasma etch to remove the exposed BOX layer. Finally, a solvent was used to release the dies from the support wafer. SEM images of the fabricated devices are shown in figure 1.

## 4. Methodology I : Strobed Raman

The principle behind method I is to strobe the Raman laser in synchronisation with the vibrating device at a fixed phase of the motion, this gives a capture of the induced strain at that phase. The phase difference between the device's motion and the laser is sequentially stepped through $2\pi$ to obtaining the strain in the device as a function of time.

### *4.1. Experimental method*

Figure 3 shows a schematic of the experimental setup. The beam from a Lynx tunable Littrow external cavity diode laser (Sacher Lasertechnik), tuned to 632.8nm, was directed via 2 mirrors into the 'superhead' of a FHR1000 Raman system (Horiba Jobin Yvon). The laser light was focussed using a 50X long working distance objective to a spot size of 4µm. The sample was mounted on a piezo disk inside a vacuum chamber (pressure of 40µbar). The piezo disk, supplied by Morgan Matroc, allowed for both in plane and out of plane actuation. XYZ staging was used to position and focus the laser. A camera system in the superhead allowed for visualisation of the beam position. The Raman signal was returned through an optical fibre into a spectrometer and detected using a liquid nitrogen cooled CCD. Data points were collected every 0.25cm$^{-1}$.

A MLD1000 controller (Sacher Lasertechnik) was used for the diode laser. Through the bias T option of the laser head, a high frequency current modulation was superimposed onto the d.c. laser current. To set an appropriate current modulation, an input frequency of $16f_0$ ($f_0$ being the resonant frequency of the device) was sent into a logic circuit, the output of which was a drive signal for the device of frequency $f_0$ and a corresponding $1/16^{th}$ duty cycle square wave pulse, the tuneable phase being set by the circuit. Additional circuitry was then used to protect the diode laser from voltage spikes. The device drive signal was amplified using a TEGAM Model 2350 high voltage amplifier.

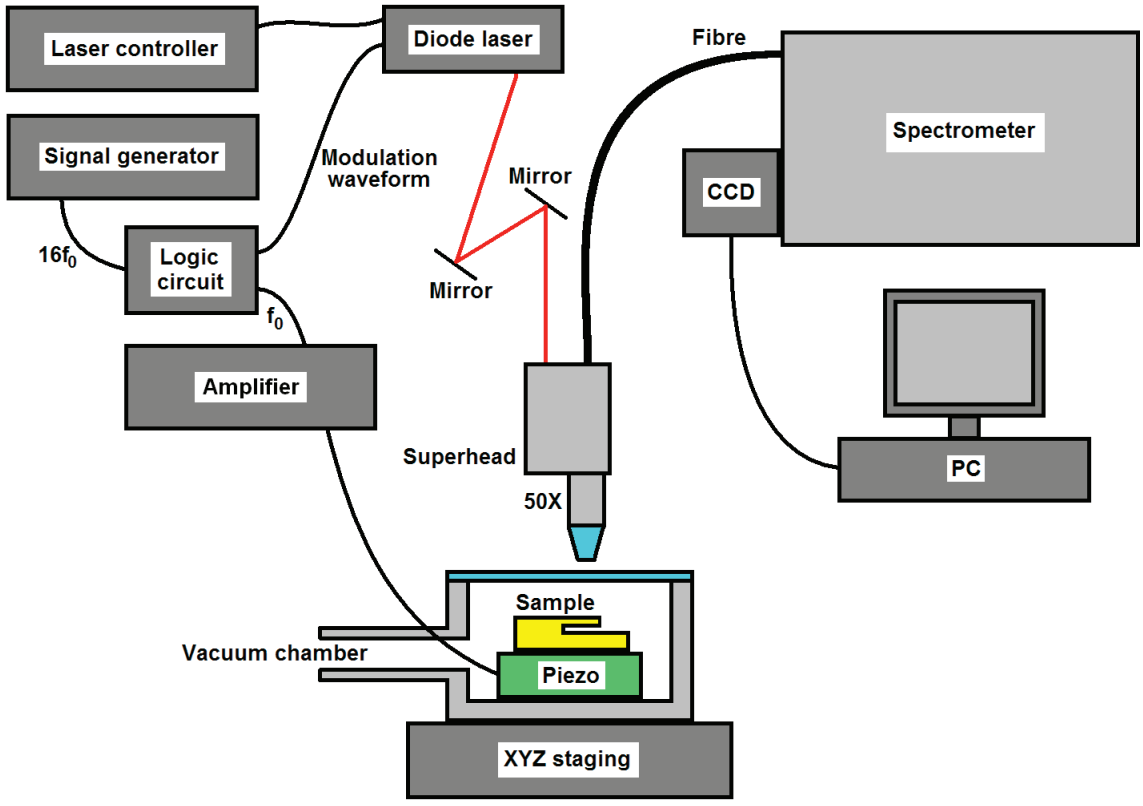


Figure 3: Schematic of the experimental setup for the strobed Raman measurements.

Figure 4(a) shows the intensity of the laser output for a base current of 60mA and modulation current of 28mA. These base and modulation currents were set to give a high on/off Raman signal ratio to allow for a 'snapshot' of the strain within the device during its motion. An average laser power of 570µW was recorded from the objective, as measured by a Coherent LaserCheck powermeter. Figure 4(b) shows the difference between a duty cycle of 1/16$^{th}$ and 0 (i.e. base current only). From this, it can be deduced that the 'off' period of the diode laser does not contribute (w.r.t. noise limits) to the Raman signal and the measured strain corresponds to only that phase of the device's motion.

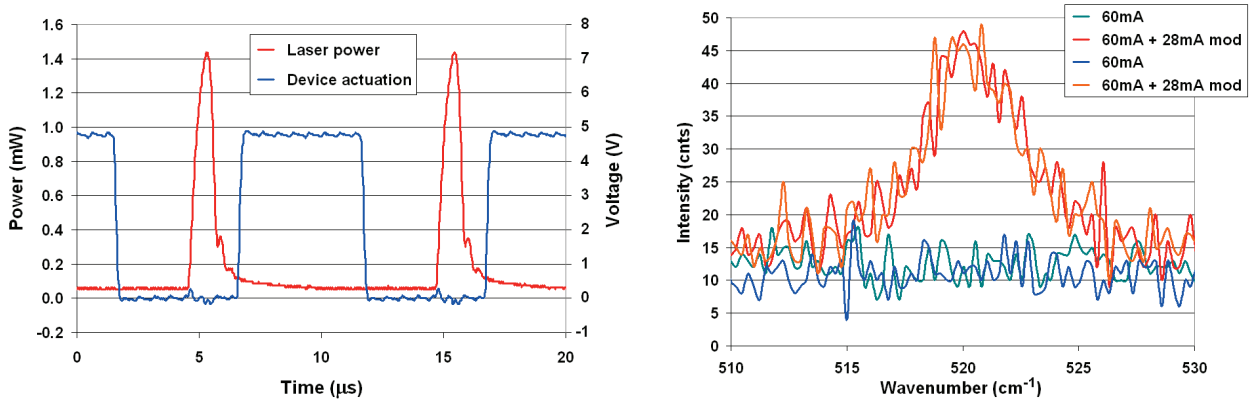


**(a)** **(b)**

Figure 4: (a) A measurement of laser intensity shows an on:off ratio of 23:1. (b) Comparison of Raman profile obtained from 1/16$^{th}$ and 0 duty cycles.

Each device was driven into resonance and the strobed Raman measurements taken at the 16 phase angles. As the duty cycle reduces the average intensity of the laser, each profile required a measurement time of 50 seconds. Figure 5 shows typical profiles obtained at differing phase positions.

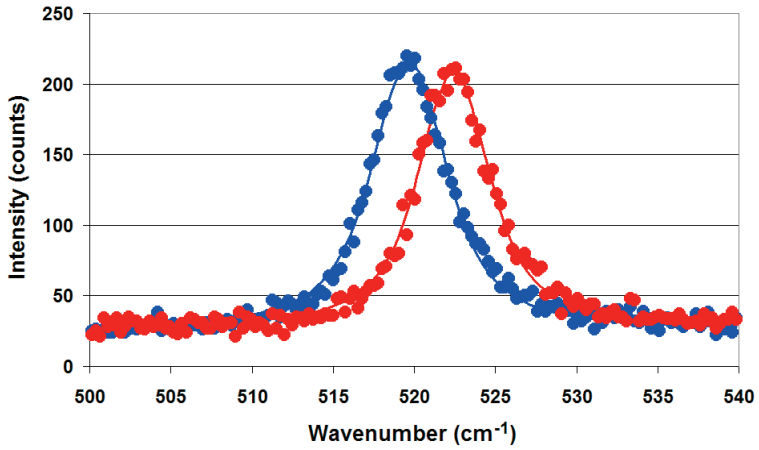


Figure 5: Raman profile obtained at 2 phases of the device's motion (corresponding to positions 135$^0$ and 292.5$^0$ in figure 6).

*4.2. Results and Discussion*

Figure 6 shows the fitted peak positions of Raman measurements taken on a triangular shaped cantilever as shown in figure 1a. Measurements were taken at the root mid-width, as indicated in the figure. The device was driven at its fundamental out of plane resonance of 98.7 KHz. Fitting of a sine wave to the data indicated a wavenumber shift amplitude of 1.47, scaling [14] to a dynamically induced strain of ±2830 µstrain.

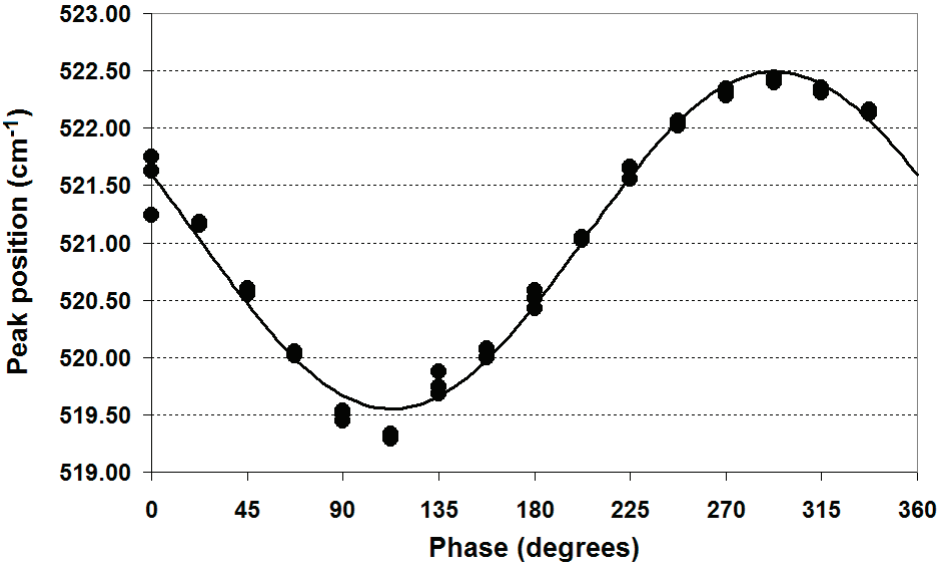


Figure 6: Peak position of the silicon Raman peak during resonance.

To estimate the accuracy of the technique, 24 measurements were taken with the device driven off resonance, off resonance being used so that any spatial drift did not affect the measurement. An average peak position of 520.56 $cm^{-1}$ was obtained with standard deviation of 0.11, this deviation scaling to 210 µstrain. Even though the laser head was temperature controlled, temperature drift was noticeable. Figure 7 shows a succession of measurements taken at various phase positions. It is evident that laser drift occurred during the initial measurements. This laser stability ultimately limits the accuracy of the method in this experiment.

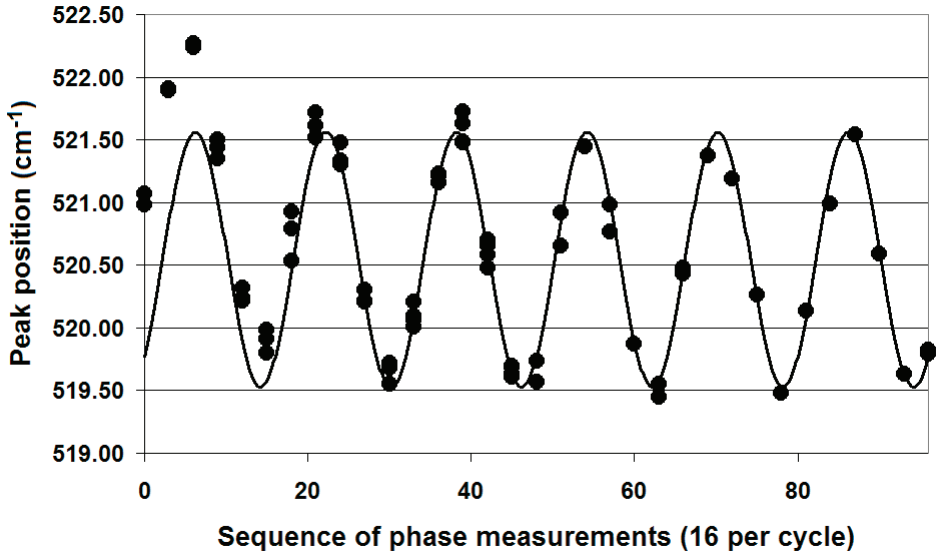


Figure 7: The poor fit of the initial experimental data points indicate drift in the laser's wavelength.

**5. Methodology II : Profile broadening**

The principle behind method II is to continuously record the Raman spectra as the device vibrates. As the camera operates at a much lower frequency than the device (<1KHz compared to > 10KHz), the effect is to spread the profile over a larger wavenumber range. A measure of this widening gives a measure of the strain induced during the vibration. Figure 8 illustrates the technique by showing

two Raman profiles, one with no dynamic strain (denoted '○') and one taken when the device was driven at its resonant frequency of 183KHz (denoted '□').

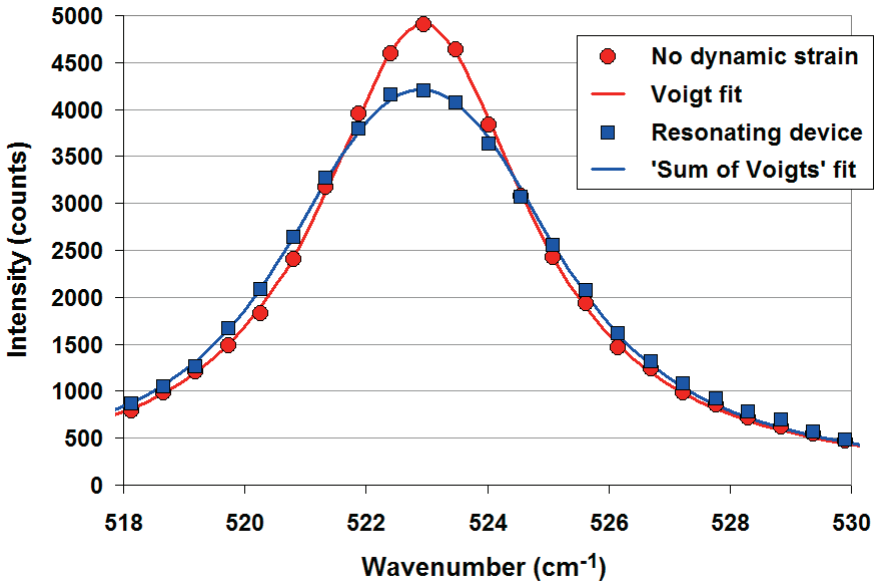


Figure 8: The Raman profile of silicon appears broadened during resonance.

*5.1. Experimental method*

For this experiment, an unmodified Horiba Jobin Yvon HR800 Raman system utilising a 514nm $Ar^+$ laser probe beam was used with 5.2mW being delivered to the silicon surface. The system comprised of a motorised xy stage which allowed for automated mapping. The device was again actuated with a piezo disk however due to the limited working volume in this Raman system, this time the device was operated in atmospheric pressure. A 100X objective was used to image the device and collect the Raman signal, this gave a diffraction limited resolution of 1μm. The Raman signal was passed through the spectrometer before being measured by a CCD camera, data points being collected every 0.54$cm^{-1}$. The profile was then saved to PC. Each profile took 1 second to collect.

To determine the reference profile from which broadening would be measured, Raman spectra were recorded in the region around the clamped end of the device whilst the device was motionless. A Voigt profile, $V(\bar{\upsilon}_0)$, was fit to this 'static' profile using a non linear least squares fitting routine, the 5 fitted parameters being the Gaussian and Lorentzian widths, wavenumber of peak position $(\bar{\upsilon}_0)$, intensity scaling factor and background level. The piezo actuator was then used to drive the device into resonance and Raman spectra were taken in the area around the clamped end, as shown in figure 1(b).

The Raman profile, R, obtained whilst the device was in motion is given by the sum of the Voigt profiles with peak positions being a function of time over the oscillation period P:

$$R \propto \int_P V(\bar{\upsilon}_0(t)). \tag{8}$$

The peak position varies sinusoidal as the device's vibration produces a periodic compression and tensioning of the crystal lattice. The maximum wavenumber shift is determined by the maximum of the volumetric strain multiplied by the calibration factor and can be defined by parameter $A_0$. The expected Raman profile may therefore be written as:

$$R \propto \sum_{n=1}^{N} V\left(\bar{\upsilon}_0 - A_0 \sin\left(\frac{2\pi n}{N}\right)\right). \tag{9}$$

Again, a non linear least squares fitting routine function was used with the sum, *N*, being taken over 16 points in the period. Using more points than this did not affect the final values but significantly increased the fitting time. For these fits, the Gaussian and Lorenztian widths were held constant at the values previously determined. The maximum shift ($A_0$), peak position, intensity scaling and background parameters were fit. The peak position was fit to account for any residual static strains in the device layer of the wafer due to fabrication. Again, the calibration factor given in [14] was used to convert $A_0$ from wavenumber to volumetric strain.

*5.2. Results and discussion*

An array of data points were taken around the clamped region of the device, the finite element modelling of this region is shown in figure 9. Maps of the recorded volumetric strain, as measured through the broadening of the Raman profile during vibration, are shown in figure 10. Note only data points with an intensity fitted parameter of at least 66% of those points located at the centre of the device were used, points of lower intensity were defined as being off the device, out of focus and hence not relevant to this analysis. The strain contours indicate the mode shape of the vibration, as compared with the finite element modelling. A higher spatial resolution map recorded around the highly strained fillet of the clamped end is also shown. The measured strain maps clearly show regions of high strain induced in the device as it vibrates.

Note that to map this strain along the length of a device of this size vibrating at micron sized amplitudes would be problematic as out of plane motion would invoke focussing problems and in plane motion would make spatial alignment of the laser impossible. Mapping of these devices is therefore limited to the area around nodal regions.

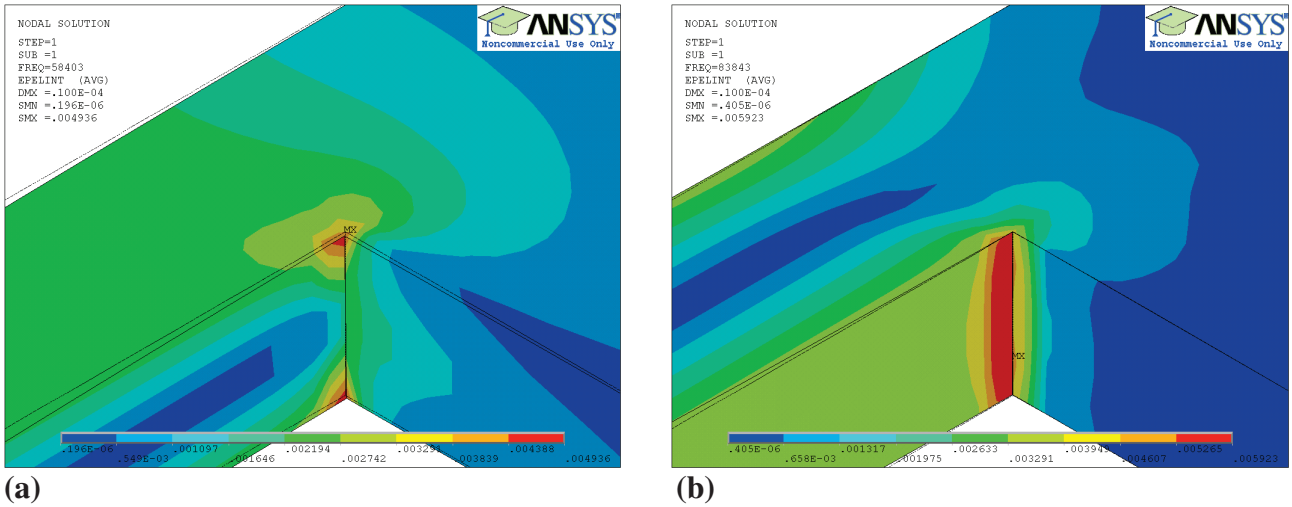


**(a)** **(b)**

Figure 9: Modelled strain intensity maps of a test structure showing (a) first out of plane and (b) first in plane mode of vibration for a free end amplitude of 10µm.

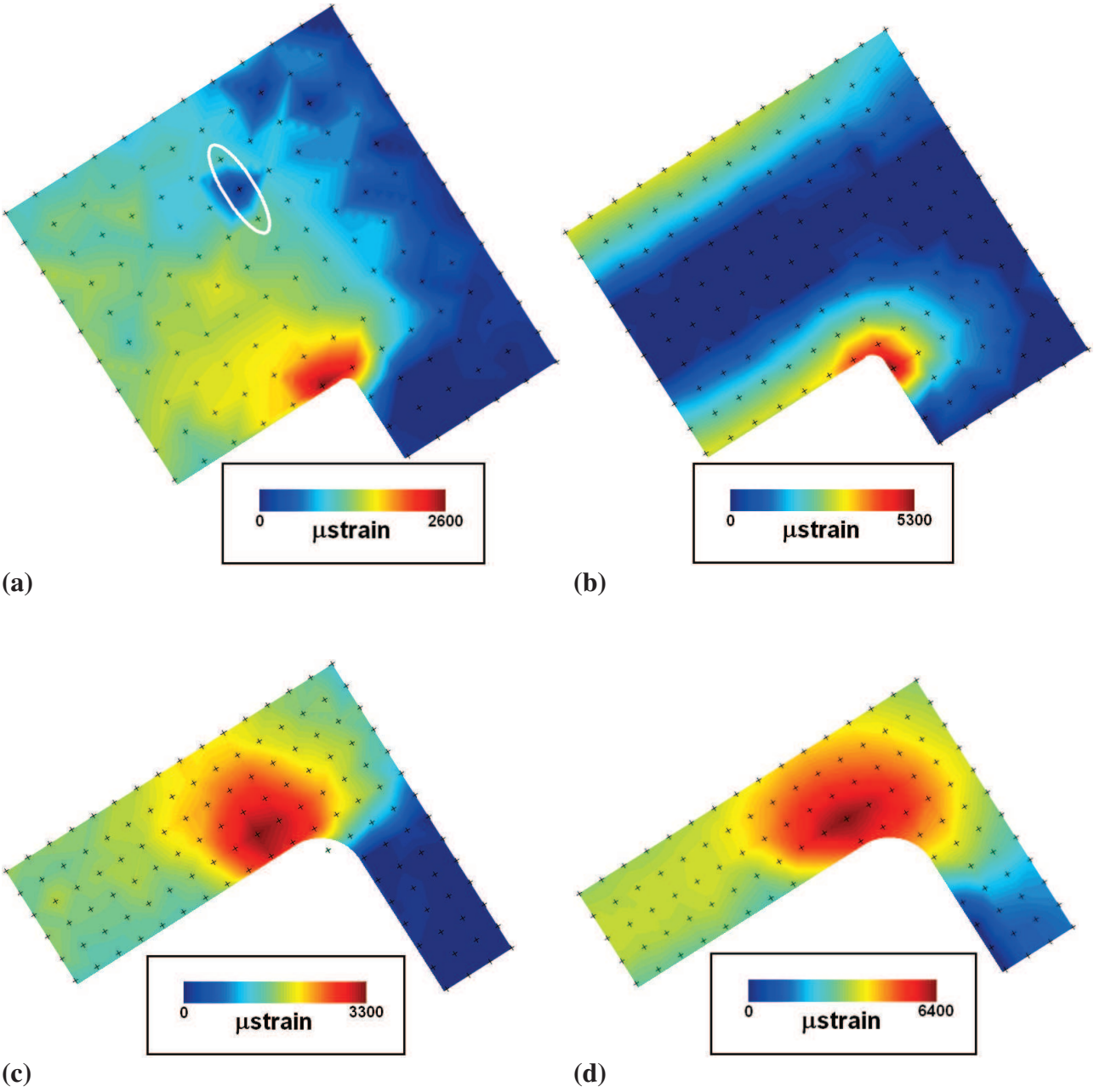


Figure 10: Strain induced during oscillation in (a) the first out of plane and (b) first in plane modes of vibration. Crosses indicate measurement points every 2µm. For each mode, corresponding high spatial resolution maps (points every 500nm) are shown in (c) and (d) respectively.

Anomalies of strain appear in the maps, for example the highlighted points in figure 10(a). There are two possible reasons for this. Firstly the silicon lattice may be disrupted causing these spurious points. A Raman mapping of the device whilst it is stationary would clarify this. Alternatively, Raman profiles are notorious for spikes in the data which can significantly affect the fitting procedure, as is the case here. One way to detect this would be to take multiple measurements at each location, the drawback being a significant increase in measurement time. An alternative solution is to analyse each profile twice, using half of the data set in each case (i.e. every second point). This is illustrated in table 1 and clearly shows where a ‘good’ point shows a 10% deviation in the fit of the width whilst the spurious point shows several orders of magnitude variation between the fits. Only the ‘poor’ data points would then require a re-measurement. Note that in figure 10, the original data is shown, a re-measurement was not performed here as data was analysed off-line at a later date.

Table 1: Fitting parameters for the 3 highlighted data points (as indicated in figure 10(a)) using various selections of the data.

| Data point (as viewed) | Data fitted (%) | Width $(\overline{\upsilon})$ | Intensity (cnts $\times 10^3$) | Background (cnts) | Peak $(\overline{\upsilon})$ | Sum of squares ($\times 10^3$) |
|---|---|---|---|---|---|---|
| Upper | 100 | 0.6403 | 2.95 | 24 | 522.71 | 41.6 |
| | 50 | 0.6459 | 2.91 | 24 | 522.73 | 17.8 |
| | 50 | 0.6526 | 2.96 | 24 | 522.69 | 19.6 |
| Middle | 100 | 0.0005 | 3.11 | 29 | 522.71 | 40.9 |
| | 50 | 0.0231 | 3.10 | 27 | 522.72 | 15.9 |
| | 50 | 0.4354 | 3.11 | 24 | 522.71 | 21.3 |
| Lower | 100 | 0.5704 | 3.05 | 25 | 522.70 | 39.6 |
| | 50 | 0.6086 | 3.04 | 24 | 522.71 | 19.8 |
| | 50 | 0.5417 | 3.05 | 25 | 522.69 | 19.0 |

Due to the high amplitudes of vibration used in this experiment, fatigue in this mapped device resulted in fracture occurring shortly after the mapping was performed, the point of crack initiation occurring at the predicted and measured high strain locations. Figure 11 is an SEM of the device mapped in figure 10 after failure during in plane oscillation. The high strain points occur on both the top and bottom surfaces and in this case, the lower surface produced the initiation point. However the image does indicate the onset of failure on the upper surface and illustrates the potential of this Raman mapping for reliability studies of MEMS. Note that real time imaging of a failure as it rapidly propagates remains problematic due to the finite time required to perform a measurement and move the staging.

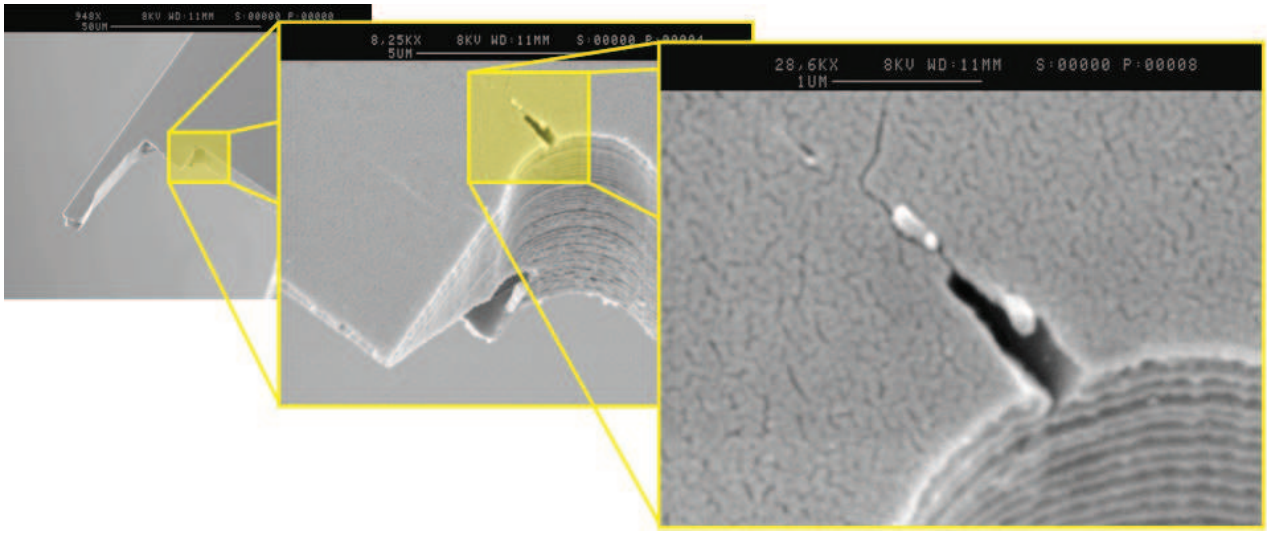


Figure 11: SEM images of the fractured device due to excessive in plane vibration.

Displacement measurements on similar devices, using a Zygo NewView 5020 dynamic profiler and Polytec OVF512 laser vibrometry, showed vibration amplitudes and corresponding predicted strain levels of the same order before fracture. Table 2 summarizes volumetric strain levels from the different approaches. Both peak and peak average over $3\mu m^3$ (corresponding to the Raman measurement volume for a penetration depth of 3µm) are given. The variation between devices demonstrates the need for a direct measurement of strain.

Table 2: Comparison of directly and indirectly measured strains induced during vibration.

| # | Frequency (KHz) | Technique | Actuation (V) | End disp. (um) | Peak volumetric strain (μstrain) | | | |
|---|---|---|---|---|---|---|---|---|
| | | | | | Measured | FEA $3\mu m^3$ | FEA peak | Analytical peak** |
| Out of plane fundamental | | | | | | | | |
| 1 | 63.98 | Raman | 60 | - | 3320 | - | - | - |
| 2 | 63.56 | Laser vibrometry | 60 | 7.0 | - | 1150 | 1470 | 1540 |
| 3 | 63.85 | | 60 | 15.5 | - | 2550 | 3260 | 3400 |
| 4 | 64.17 | | 50 | 18.0 | - | 2960 | 3790 | 3930 |
| In plane fundamental | | | | | | | | |
| 1 | 91.38 | Raman | 60 | -* | 6410 | - | - | - |
| 2 | 89.40 | Dynamic profiler | 40 | 23.5 | - | 7220 | 9510 | 7120 |
| 3 | 90.77 | | 30 | 31.1* | - | 9590 | 12600 | 9280 |
| 4 | 90.56 | | 35 | 18.8* | - | 5790 | 7620 | 5750 |

* Fractured

** Stress concentration factor not included

## 6. Conclusions

This work has compared two approaches in utilising Raman spectroscopy as a way to characterise silicon MEMS devices. As the technique is a point measurement, characterisation is slow compared with alternative optical methodologies and measurements must be performed around nodal regions. However the technique is shown to be a 3-dimensional characterisation technique with the ability of characterising the combination of both out of plane and in plane motions. Additionally, as the technique utilises the crystal lattice as the reference frame, featureless regions of devices may be characterised. This has potential advantages over feature tracking techniques, for example, to highlight discontinuities due to lattice inhomogeneities caused by dislocations or implantations.

For this experiment, the 30μstrain measurement resolution limit corresponds to a minimum measurable device vibration amplitude of 350nm and therefore alternative optical characterisation techniques such as laser vibrometry and surface profilometry are significantly more sensitive for displacement measurements of these devices. However, as strain is proportional to the curvature of the mode shape, the Raman technique approaches the sub-nanometre sensitivities of conventional optical techniques as device dimensions are reduced and higher order modes are examined. For example, a silicon cantilever of dimensions 2000(l)×170(w)×300(t)nm would theoretically experience 30μstrain for a fundamental mode amplitude of 0.8nm.

The Raman technique does offer a direct measure of strain and as it relies on scattered rather than reflected light, lends itself to high spatial resolution measurements through tip enhancement techniques. The work has also demonstrated the potential of utilising the technique for the increasing need of reliability studies on MEMS devices, the strain maps produced giving an indication of possible locations of device failure.

**Acknowledgements**

The authors wish to acknowledge and thank EPSRC for research grant EP/C015045/1. The authors also thank Barry Dunn (INEX, Newcastle University) for fabrication of the devices and Tracey Davey (EM Research Services, Newcastle University) for the SEM imaging.

## References

[1] A. Bosseboeuf and S. Petitgrand, *Journal of Micromechanics and Microengineering* **13** (2003) S23-S33.
[2] J. S. Burdess, A. J. Harris, D. Wood, R. J. Pitcher and D. Glennie, *Journal of Microelectromechanical Systems* **6** (1997) 322-328.
[3] C. Q. Davis and D. M. Freeman, *Optical Engineering* **37** (1998) 1299-1304.
[4] M. R. Hart, R. A. Conant, K. Y. Lau and R. S. Muller, *Journal of Microelectromechanical Systems* **9** (2000) 409-418.
[5] P. Aswendt, C-D. Schmidt, D. Zielke and S. Schubert, *Optics and Lasers in Engineering* **40** (2003) 501-515.
[6] W. Merlijn van Spengen, R. Puers, R. Mertens and I. De Wolf, *Microsystems Technologies* **10** (2004) 89-96.
[7] D. J. Burns and H. F. Helbig, *Journal of Microelectromechanical Systems* **8** (1999) 473-482.
[8] J. Hedley, A. J. Harris and J. S. Burdess, *Proceedings of SPIE* **4408** (2001) 402-408.
[9] C. Rembe and R. S. Muller, *Journal of Microelectromechanical Systems* **11** (2002) 479-488.
[10] C. L. Muhlstein, S. B. Brown and R. O. Ritchie, *Journal of Microelectromechanical Systems* **10** (2001) 593-600.
[11] I. De Wolf, *Semiconductor Science Technology* **11** (1996) 139-154.
[12] M. Bowden and D. J. Gardiner, *Applied Spectroscopy* **51** (1997) 1405-1409.
[13] M. A. Lourenco, D. J. Gardiner, M. Bowden, J. Hedley and D. Wood, *Journal of Materials Science Letters* **19** (2000) 767-769.
[14] M. Bowden, D. J. Gardiner, D. Wood, J. Burdess, A. Harris and J. Hedley, *Journal of Micromechanics and Microengineering* **11** (2001) 7-12.
[15] V. T. Srikar, A. K. Swan, M. S. Ünlü, B. B Goldberg and S. M. Spearing, *Journal of Microelectromechanical Systems* **12** (2003) 779-787.
[16] S. Webster, D. N. Batchelder and D. A. Smith, *Applied Physics Letters* **72** (1998) 1478-1480.
[17] C. Xue, L. Zheng, W. Zhang, B. Zhang and A. Jian, *Journal of Raman Spectroscopy* **38** (2007) 467-471.
[18] J. Hedley, Z. X. Hu, I. Arce_Garcia and B. J. Gallacher, *Proceedings of the 3rd IEEE International Conference on Nano/Micro Engineered and Molecular Systems* (Sanya, 2008) 842-846.
[19] R. Loudon, *Advances in Physics* **13** (1964) 423-482.
[20] E. Anastassakis, A. Pinczuk and E. Burstein, *Solid State Communications* **8** (1970) 133-138.
[21] S. Narayana, S. R. Kalidindi and L. S. Schadler, *Journal of Applied Physics* **82** (1997) 2595-2602.
[22] S.S. Rao, *Mechanics of Vibration* (Pearson, Prentice Hall, 2005) 545.
[23] W. D. Pilkey, *Peterson's Stress Concentration Factors, 2nd edition* (John Wiley & Sons, 1997) Chapter 3.